Evidence of spin transition and charge order in cobalt substituted $La_{0.7}Ca_{0.3}MnO_3$

2003 J. Phys.: Condens. Matter 15 2375

(http://iopscience.iop.org/0953-8984/15/14/313)

INSTITUTE OF PHYSICS PUBLISHING JOURNAL OF PHYSICS: CONDENSED MATTER

J. Phys.: Condens. Matter **15** (2003) 2375–2388 PII: S0953-8984(03)57843-2

Evidence of spin transition and charge order in cobalt substituted $La_{0.7}Ca_{0.3}MnO_3$

C M Srivastava[1], Santanu Banerjee[2], T K GunduRao[3], A K Nigam[4] and D Bahadur[2,5]

[1] Department of Physics, IIT Bombay, Powai, Mumbai-400076, India
[2] Department of Metallurgical Engineering and Materials Science, IIT Bombay, Powai, Mumbai-400076, India
[3] Regional Sophisticated Instrumentation Center, IIT Bombay, Powai, Mumbai-400076, India
[4] Tata Institute of Fundamental Research, Colaba, Mumbai-400005, India

Received 6 January 2003
Published 31 March 2003
Online at stacks.iop.org/JPhysCM/15/2375

Abstract

The transport and magnetic studies of a series of compounds having the general formula $La_{0.7}Ca_{0.3}Mn_{1-x}Co_xO_3$ ($0.1 \leqslant x < 0.9$) have shown that Co^{3+} can exist both in high spin and low spin states (diamagnetic state). This is found to affect greatly the transport and magnetic properties of the system at low temperature by varying the strengths of both double-exchange (DE) and superexchange (SE) interactions. The introduction of cobalt changes the mobile carrier concentration, so even with 10% of Co concentration the strength of DE is found to decrease considerably. For $x \geqslant 0.25$ there is a clear spin transition at low temperature from the high to the low spin state of trivalent cobalt and this leads to change in ferromagnetic (FM) and antiferromagnetic (AFM) phases. For $x \geqslant 0.25$ there are two transitions for each value of x: the upper one gives the FM and AFM spin arrangement depending upon whether the DE or the SE dominates; the lower one is obtained due to the transition from the high to the low spin state of the trivalent cobalt ion.

1. Introduction

In the recent past the substituted perovskite manganites have drawn attention due to their well known colossal magnetoresistance (CMR) property. The partial substitution with bivalent and trivalent cations for R in $RMnO_3$ leads to the existence of mixed valence states of Mn^{3+} and Mn^{4+} ions which through the 'double exchange (DE)' interaction leads to CMR and other interesting properties [1–3]. The extent of substitution with bivalent and trivalent cations affects the magnetic and electrical transport behaviour and the system can behave as an antiferromagnetic insulator (AFI), ferromagnetic (FM) metal, ferromagnetic

[5] Author to whom any correspondence should be addressed.

insulator (FI) and paramagnetic insulator (PI) [4–9]. For manganites of general formula $R_{1-y}A_yMnO_3$ (A = Ca, Sr, Ba) there is a metal–insulator transition for $0.2 < y < 0.5$ which is also associated with the FM to paramagnetic (PM) transition. For all these mixed valent manganites both the ferromagnetism and the mechanism of CMR have been traditionally explained by means of the DE model which describes the magnetic coupling between Mn^{3+} and Mn^{4+} ions resulting from the transfer of an e_g electron between two partially filled d orbitals. Hence the electron transport is closely associated with the magnetic states that vary with temperature and externally applied magnetic field. In recent studies it has been observed that several other factors like local Jahn–Teller distortion of Mn^{3+} ions [10] affect the physical properties of these systems.

In our present system we have studied the effect of the presence of two transition metal ions like Mn and Co on B sites both of which can exist in mixed valent states. The interesting question is whether DE can take place between the two different transition metal ions. There are reports of such an interaction occurring in Ni^{3+}–O–Co^{3+} [11] and Mn^{3+}–O–Cr^{3+} [12]. Among the Mn and Co ions present in the system the transfer of the single e_g electron of the $Mn^{3+}(t_{2g}^3e_g^1)$ ion to the vacant e_g orbital of the low spin Co^{III} $(t_{2g}^6e_g^0)$ ion is possible. It has been observed that the Mn site doping in $R_{1-y}A_yMnO_3$ with Co has spectacular effects in both magnetic and transport properties. In fact, it is reported that there is a transition from the insulating antiferromagnet to the metallic ferromagnet phase in $Pr_{0.5}Ca_{0.5}Mn_{1-x}M_xO_3$ with M = Cr and Co when x is increased from 0 to as small a value as 0.02 [13]. The mechanism of I–M transition and the associated changes in magnetic ordering on Co/Cr doping are not well understood. We have therefore carried out a study of the $La_{0.7}Ca_{0.3}Mn_{1-x}Co_xO_3$ system for $0.1 \leqslant x \leqslant 0.9$.

2. Experimental details

The solid solution of cobaltite and manganite having the general formula $La_{0.7}Ca_{0.3}Mn_{1-x}Co_xO_3$($x = 0.1, 0.2, 0.25, 0.3, 0.4, 0.5, 0.7, 0.9$) has been synthesized using the chemical citrate gel route. X-ray diffractograms of the prepared samples were recorded using an x-ray diffractometer (Philips PW1710). All the samples were found as polycrystalline single perovskite phase. The variation of magnetization with temperature for the samples was measured using vibrating sample magnetometer (Oxford VSM) in a magnetic field of 4 kOe and in the temperature range of 4–300 K. Resistivity measurement was made from 300 to 10 K using the standard four-probe method with the help of a Keithley nanovoltmeter (type 181) and a Keithley auto-tuning programmable current source (type 224) using a Lakeshore close cycle system (CTI, Cryogenics, Helix Technology Corporation) and temperature controller (type 330).

3. Results

3.1. Resistivity

The plots of the temperature dependence of resistivity, $\rho(T)$, for $La_{0.7}Ca_{0.3}Mn_{1-x}Co_xO_3$ ($0.1 \leqslant x \leqslant 0.5$) are shown in figure 1. For $x = 0.7$ and 0.9 the curves are essentially similar to $x = 0.5$ and so have not been included. The following features of the curves are noticeable.

(i) The room temperature resistivity (300 K) is lowest for $x = 0.25$ and is highest for 0.1.
(ii) The resistivity for $0.1 \leqslant x \leqslant 0.4$ shows a peak at temperature T_c^p, which generally decreases as x is increased (table 1). The resistivity for $x = 0.5$ increases continuously as the temperature is decreased.

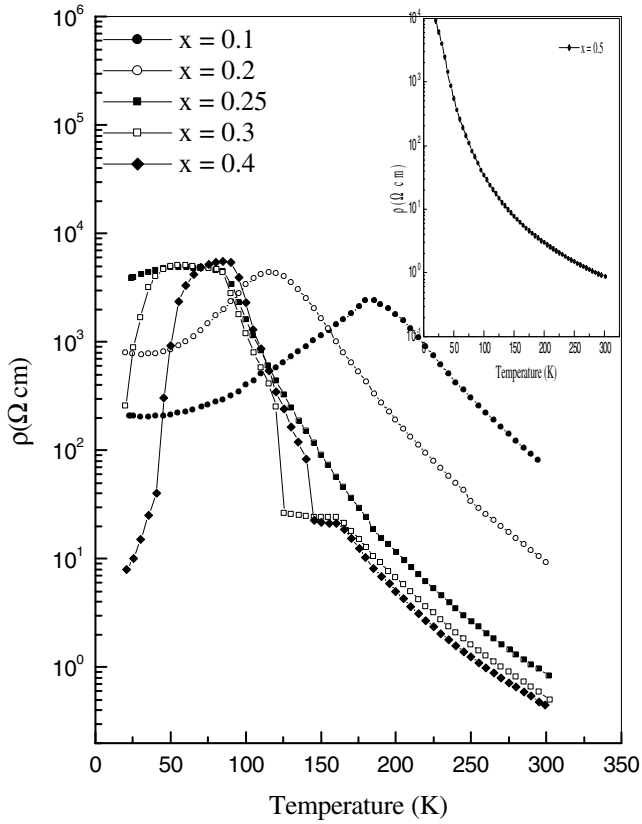

Figure 1. The variation of resistivity with temperature for $0.1 \leqslant x \leqslant 0.5$ in $La_{0.7}Ca_{0.3}Mn_{1-x}Co_xO_3$. The curve for $x = 0.5$ is given in the inset.

Table 1. The parameters used to fit the $\rho(T)$ data of $La_{0.7}Ca_{0.3}Mn_{1-x}Co_xO_3$ ($0.1 \leqslant x \leqslant 0.5$) using equation (3) (see the text). The phonon frequency $\upsilon_{ph} = 5 \times 10^{12}$ Hz, $a = 3.858$ Å. T_c is taken from table 2 and $T_{ca} = 350$ K. Other parameters are chosen to get the best fit to the $\rho(T)$ curves. T_c^p is the temperature at which the peak in resistivity is observed. ρ_{0A} is the value in equation (4) at which $\varepsilon_p' = 60$ K, $T_c' = 90$ K, $m(t') = 1$ and $\theta = 20$ K for $0.1 \leqslant x \leqslant 0.4$. n is the number of charge carriers, ε_p is the value of the small polaron stabilization energy and U_0 is the activation energy in equation (1).

x	A/n (10^{-4} Ω cm K^{-1})	n (10^{19} cm^{-3})	ε_p (K)	U_0 (K)	T_c^p (K)	T_c (K)	ρ_{0A} (Ω cm)
0.10	150	0.54	400	1150	185	220	150
0.20	25	3.2	400	1000	125	206	1500
0.25	5	16.4	200	800	85	188	2500
0.30	4	20.4	200	650	75	177	4000
0.40	3	27.3	200	750	85	170	2500
0.50	12	6.8	180	480	—	177	—

(iii) The low temperature resistivity for $x = 0.1$ and 0.2 shows a small upturn while for $x = 0.25$, 0.3 and 0.4 it shows a downturn.

(iv) The peak resistivity is nearly the same for $0.1 \leqslant x \leqslant 0.4$ and lies between 2×10^3 and 5×10^3 Ω cm.

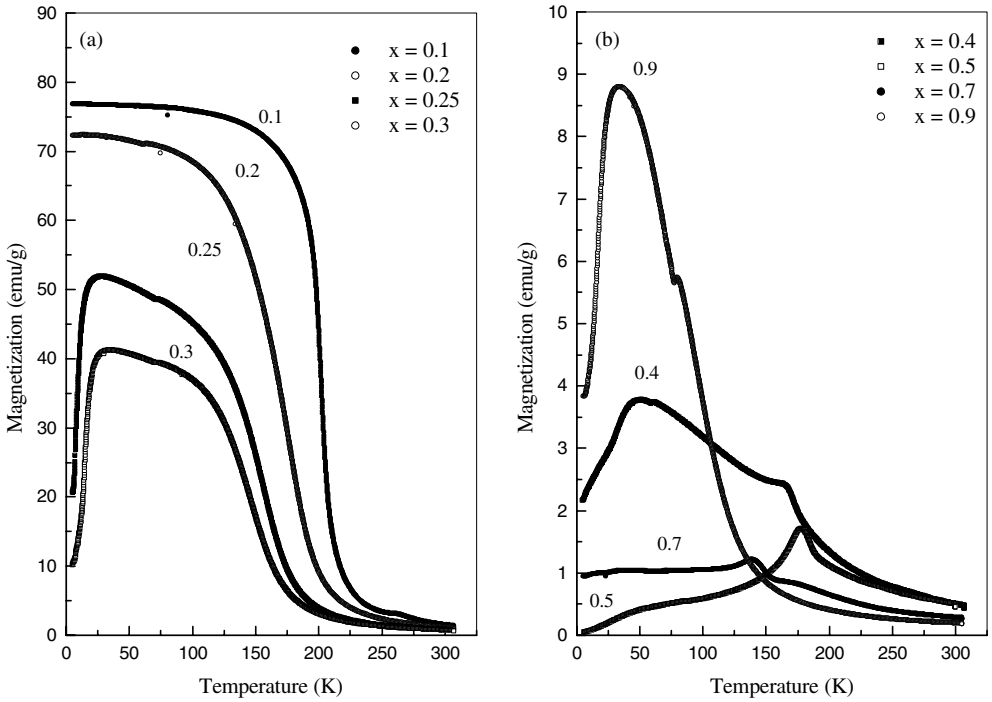

Figure 2. The variation of magnetization, $M(T)$, with temperature for $0.1 \leqslant x \leqslant 0.5$ in $La_{0.7}Ca_{0.3}Mn_{1-x}Co_xO_3$: (a) $x = 0.1$, 0.2, 0.25 and 0.3; (b) $x = 0.4$, 0.5, 0.7 and 0.9.

These features are in sharp contrast to the resistivity curve for pure LCMO, $La_{0.7}Ca_{0.3}MnO_3$, for which T_c^p is close to T_c, the Curie point, and $\rho(300\,\mathrm{K})$, $\rho(T_c^p)$, $\rho(10\,\mathrm{K})$ are all in the mΩ cm range [6]. For comparison T_c obtained from magnetic data for $0.1 \leqslant x \leqslant 0.5$ is included in table 1.

3.2. Magnetization

The temperature dependence of magnetization, $M(T)$, for all samples in the range of 5–300 K is shown in figures 2(a) and (b). There is a decrease in the peak magnetization values with gradual increase in cobalt concentration. The samples with $x = 0.1$ and 0.2 have the highest peak magnetization values of 76 and 72 emu g^{-1} at 5 K respectively. The above values are less than that obtained for pure $La_{0.7}Ca_{0.3}MnO_3$ (80–90 emu g^{-1}). With x in the range of 0.25–0.9 the samples show two separate transitions in their magnetization plots; the upper critical point is from PM to FM or to antiferromagnetic (AFM) at T_C (T_N) depending on x and another from FM (AFM) at a lower critical point, T_1, at which trivalent cobalt changes from the high spin to the low spin state. For example for the sample with $x = 0.25$, T_C and T_1 are 188 and 20 K respectively. Further the peak magnetization value, M_s^p, drops significantly from 72 to 52 emu g^{-1} as x increases from 0.20 to 0.25. Also the samples with $0.25 < x < 0.4$ show the same behaviour, i.e. decrease in the peak magnetization values and gradual decrease in T_C as x is increased. For $x = 0.5$, however, the first transition occurs at 177 K and is from the PM to the AF I (type A) state, and the second transition takes place at 51 K and is from the AF I to the AF II state which is a layered AFM like A with trivalent cobalt in the low spin state. At this temperature, a metal to insulator transition takes place (figure 1). The values of M_s^p and the

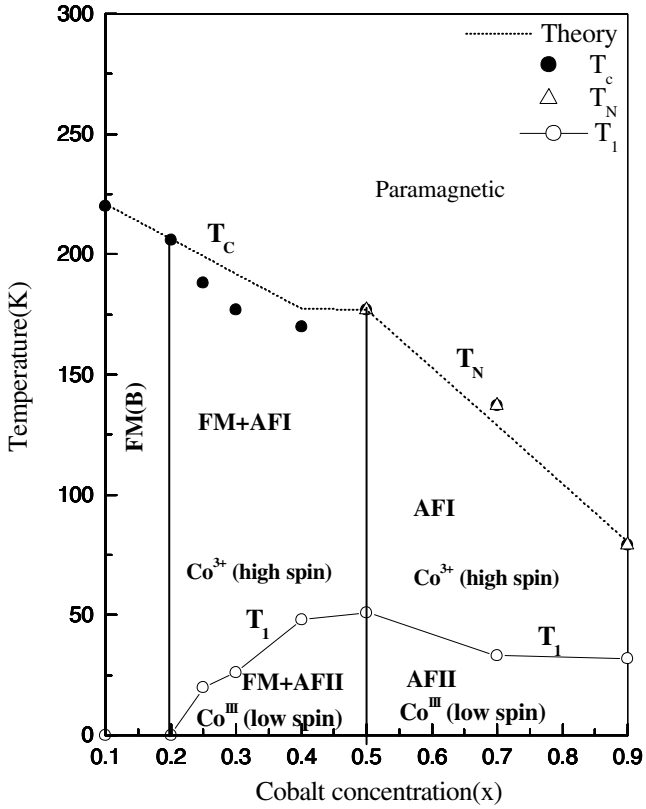

Figure 3. Magnetic phase diagram for $La_{0.7}Ca_{0.3}Mn_{1-x}Co_xO_3$ ($0.1 \leqslant x \leqslant 0.9$). The dotted line indicates the theoretical curves. The solid line indicates the experimental curve for T_1. The symbols ●, △ and ○ denote the experimental T_c, T_N and T_1 respectively. The theoretical plot (- - - -) for the upper critical point is obtained from de Gennes' expression for T_c and T_N given in equations (5) and (6) respectively (see the text). FM(B) and AFM(A) types of spin arrangement exist for $0.1 \leqslant x \leqslant 0.2$ and $0.5 \leqslant x \leqslant 0.9$ respectively and in the remaining region FM and AFM coexist. The high and the low spin trivalent cobalt states are separated by the lower critical point T_1.

magnetization at 0 K, $M_s(0)$, which are extrapolated from the 5 K data in figures 2(a) and (b), and T_c, T_N and T_1 are given in table 2. The $\rho(T)$ curves for $x = 0.7$ and 0.9 are similar to $x = 0.5$ and the M_s^p and $M_s(0)$ values are small, so in this region the upper transition from PM to AF I as x increases from 0.5 to 0.9 is gradual and smooth. This is discussed in the next section.

3.3. Magnetic phase diagram

A magnetic phase diagram has been drawn in figure 3 by plotting the experimental T_c, T_N and T_1 as a function of x which is consistent with the $\rho(T)$ data in figure 1. There are two phase boundaries. The low temperature region below T_1 forms an AFM phase which comprises of trivalent Co ions in the low spin state (Co^{III}). The transition to the high spin state occurs at the temperature T_1 when the system enters an FM phase (B) for $x \leqslant 0.4$. For $x \geqslant 0.5$, in addition to the low to high spin transition of the trivalent cobalt, the charge order also takes

Table 2. The distribution of charge and spin on each of the sublattices A_1, A_2, B_1 and B_2 for $La_{0.7}Ca_{0.3}Mn_{1-x}Co_xO_3$ ($0.1 \leqslant x \leqslant 0.9$) for the FM phase (B) and in the AFM phase (I and II) obtained from the $M(T)$ curves in figures 2(a) and (b). In AFM(I) the trivalent Co ion is in the high spin state ($t_{2g}^4e_g^2$) while in AFM(II) it is in the low spin state ($t_{2g}^6e_g^0$). Sublattice 1 comprises ions on lattice sites (000) and (aa0) and 2 on (a00) and (aaa). A indicates spin up (↑) and B spin down (↓). Each configuration of charge and spin arrangement satisfies the following: (i) four ions each on sublattices 1 and 2; (ii) the charge distribution is close to the nominal composition and (iii) the conductive phase (FM) occurs when the product of Mn^{3+} on A_1 (B_1) and Mn^{4+} on A_2 (B_2) ions is large. The number of spins like 5 ↑ for $x = 0.1$ indicates that there are five Mn^{3+} up spins distributed on $A_1(4)$ and $A_2(1)$ sublattices. M_s^p indicates the peak magnetization in the FM phase and $M_s(0)$ indicates the value of magnetization at 0 K obtained from extrapolation. The agreement between theory and experiment for M_s^p and $M_s(0)$ shows that Co changes from high spin to low spin as temperature is lowered below T_1. The possible spin arrangement type is given in the last column.

x	Phase I/ phase II	Mn^{3+} ($4\ \mu_B$)	Mn^{4+} ($3\ \mu_B$)	Co^{3+} ($4\ \mu_B$) Co^{III} ($0\ \mu_B$)	Co^{4+} ($3\ \mu_B$)	M_s^p (theo.) (emu g^{-1})	M_s^p (expt) (emu g^{-1})	$M_s(0)$ (theo.) (emu g^{-1})	$M_s(0)$ (expt) (emu g^{-1})	T_c/T_N (*)	T_1 (K)	Possible spin arrangement type
0.1	I	5.0 ↑ $A_1 + A_2$	2.0 ↑ A_2	0.50 ↓ B_2	0.50 ↓ B_2	73.38	76	73.38	76	220	—	B
0.2	I	4.5 ↑ $A_1 + A_2$	2.0 ↑ A_2	1.0 ↓ B_2	0.50 ↓ A_2	70.11	72	70.11	72	206	—	B
0.25	I	4.0 ↑ A_1	2.0 ↑ A_2	1.5 ↓ B_2	0.50 ↓ B_2	47.29	52	—	—	188	—	B
	II	2 ↑ 2 ↓ $A_1 + B_1$	2.0 ↓ B_2	1.5(0) O_2	0.50 ↑ A_2	—	—	14.67	15	—	20	A

Table 2. (Continued.)

x	Phase I/ phase II	Mn^{3+} ($4\ \mu_B$)	Mn^{4+} ($3\ \mu_B$)	Co^{3+} ($4\ \mu_B$) Co^{III} ($0\ \mu_B$)	Co^{4+} ($3\ \mu_B$)	M_s^p (theo.) (emu g^{-1})	M_s^p (expt) (emu g^{-1})	$M_s(0)$ (theo.) (emu g^{-1})	$M_s(0)$ (expt) (emu g^{-1})	$T_c/T_N(^*)$	T_1 (K)	Possible spin arrangement type
0.3	I	4.0 ↑ A_1	1.5 ↑ A_2	1.5 ↓ B_2	1.0 ↓ B_2	37.50	40	—	—	177	—	B
	II	2 ↑ 2 ↓ $A_1 + B_1$	1.5 ↑ A_2	1.5(0) O_2	1.0 ↓ B_2	—	—	4.89	5.0	—	26	A
0.4	I	3.5 ↑ A_1	0.5 ↓ 0.5 ↑ $B_2 + A_2$	2.5 ↓ B_2	1.0 ↓ B_2	3.26	3.8	—	—	170		B
	II	2 ↑ 1.5 ↓ $A_1 + B_1$	0.75 ↑ 0.25 ↓ $A_2 + B_2$	2.5(0) $O_1 + O_2$	1.0 ↓ B_2	—	—	1.63	1.75	—	48	A
0.5	I	1 ↑ 1 ↓ $A_1 + B_2$	1 ↑ 1 ↓ $A_1 + B_2$	1 ↑ 1 ↓ $A_1 + B_2$	1 ↑ 1 ↓ $A_2 + B_1$	0	1.5	—	—	177*	—	A
	II	1 ↑ 1 ↓ $A_1 + B_2$	1 ↑ 1 ↓ $A_1 + B_2$	2(0) ↓ $O_1 + O_2$	1 ↑ 1 ↓ A_2B_1	—	—	0	0	—	51	A
0.7	I	0.84 ↑ 0.84 ↓ $A_1 + B_2$	0.44 ↓ 0.28 ↑ $A_1 + B_2$	1.93 ↑ 1.99 ↓ $A_1 + B_2$	0.79 ↓ 0.89 ↑ $A_2 + B_1$	1.37	1.2	—	—	137*	—	A
	II	0.84 ↑ 0.84 ↓ $A_1 + B_2$	0.44 ↓ 0.28 ↑ $A_1 + B_2$	3.92(0) $O_1 + O_2$	0.79 ↓ 0.89 ↑ $A_2 + B_1$	—	—	0.59	1.0	—	33	A
0.9	I	0.56 ↑ A_1	0.24 ↓ A_2	1.68 ↓ 3.36 ↑ $A_1 + B_2$	1.76 ↓ 0.40 ↓ $B_1 + B_2$	11.22	8.8	—	—	77*	—	A
	II	0.56 ↑ A_1	0.24 ↑ A_2	5.04(0) $O_1 + O_2$	1.76 ↓ 0.40 ↑ $A_2 + B_2$	—	—	3.65	3.75	—	32	A

place as the population of Co ions equals or exceeds the Mn ions on the B site. Such changes in spin state have been reported in other cobaltite systems like $EuCoO_3$ and $LaCoO_3$ [14, 15]. In these systems it is suggested that cobalt ions exist predominantly in the low spin ($t_{2g}^6 e_g^0$) Co^{III} state ($^1A_{1g}$) at low temperatures and transform to the high spin state ($t_{2g}^4 e_g^2$) Co^{3+} state ($^3T_{2g}$) gradually up to ~200 K. For $x = 0.5$ the region AF I ($T_1 < T < T_N$) is semiconducting but AF II ($0 < T < T_1$) is insulating (figure 1). The transition for $x = 0.4$ at T_1 is predominantly from FM + AF I to FM + AF II. This is indicated in the $\rho(T)$ curve at low temperature as discussed in the next section. In section 4 we have shown that a low spin to high spin transition affects the strengths of the superexchange (SE) and DE interactions as well as M_s^p and $M_s(0)$ and accounts for the observed phase diagram.

4. Discussion

We now attempt to analyse the results discussed in section 3.

4.1. Resistivity

The data on resistivity have been examined using the dc hopping resistivity based on the correlated small-polaron model discussed in [16]. This gives the expression for resistivity as

$$\rho_{\text{hop}}^c = \frac{AT}{n}[1 + \{1 - m^2(t)\}\sigma_a^2] \cosh^2\left(\frac{\varepsilon_p}{2(T+\theta)}\right) \exp\left(\frac{U}{T}\right) \tag{1}$$

where

$$A = \frac{1.13 k_B}{v_{\text{ph}} a^2 e^2}. \tag{2}$$

Here n is the density of charge carriers, v_{ph} is the frequency of the longitudinal phonon mode to which the electron with charge e is coupled, a is the distance of the hop and $m(t)$ ($=M(T)/M(0)$) is the normalized magnetization at the normalized temperature, $t = T/T_c^p$. Here T_c^p is the temperature at which the peak resistivity occurs. This is different from T_c obtained from the magnetic data (table 1). σ_a is the short range order parameter, ε_p is the small polaron stabilization energy and U is the activation energy of the charge carriers, $U = U_0\xi^2$, where $\xi^2 = S_a^2(1 - S_m)^2\sigma_a^2$. Here U_0 is a constant, S_a and σ_a are the long range and short range atomic order parameters and S_m is the long range magnetic order parameter. In the present case the resistivity data fit to the following: $S_a^2 = 1$, $\sigma_a^2 = (1 - 0.75t_{\text{ca}}^3)^{1/2}$ and $(1 - S_m)^2 = (1 - m^{4.5})$. Here $t_{\text{ca}} = T/T_{\text{ca}}$ [16] and m is obtained solving $m = \tanh(m/t)$, appropriate for a system which has only two stable states, $S_z = \pm S$. In equation (2) we have taken $v_{\text{ph}} = 5 \times 10^{12}$ Hz and $a = 3.858$ Å.

Equation (1) gives the expression for resistivity when spin and phonon scattering are dominant in the B type of spin order [16]. On cobalt substitution an additional contribution comes from Co^{3+} ions which nucleate the A type of insulating phase. We then have [16]

$$\bar{\rho} = \rho(T) + \rho^*(T) \tag{3}$$

$$\rho^*(T) = \begin{cases} \rho_{0A} m^2(t') \cosh^2\left(\dfrac{\varepsilon_p'}{2(T+\theta)}\right) & T \leqslant T_c' \\ 0 & T > T_c' \end{cases} \tag{4}$$

and $\rho(T)$ applies for $T \leqslant 300$ K. Here θ has been added to T in the cosh term in equations (1) and (4) to take into account the zero point vibrations of atom which prevent complete localization of the polaron as $T \to 0$. For $0.1 \leqslant x \leqslant 0.4$ we find $T_c' = 90$ K,

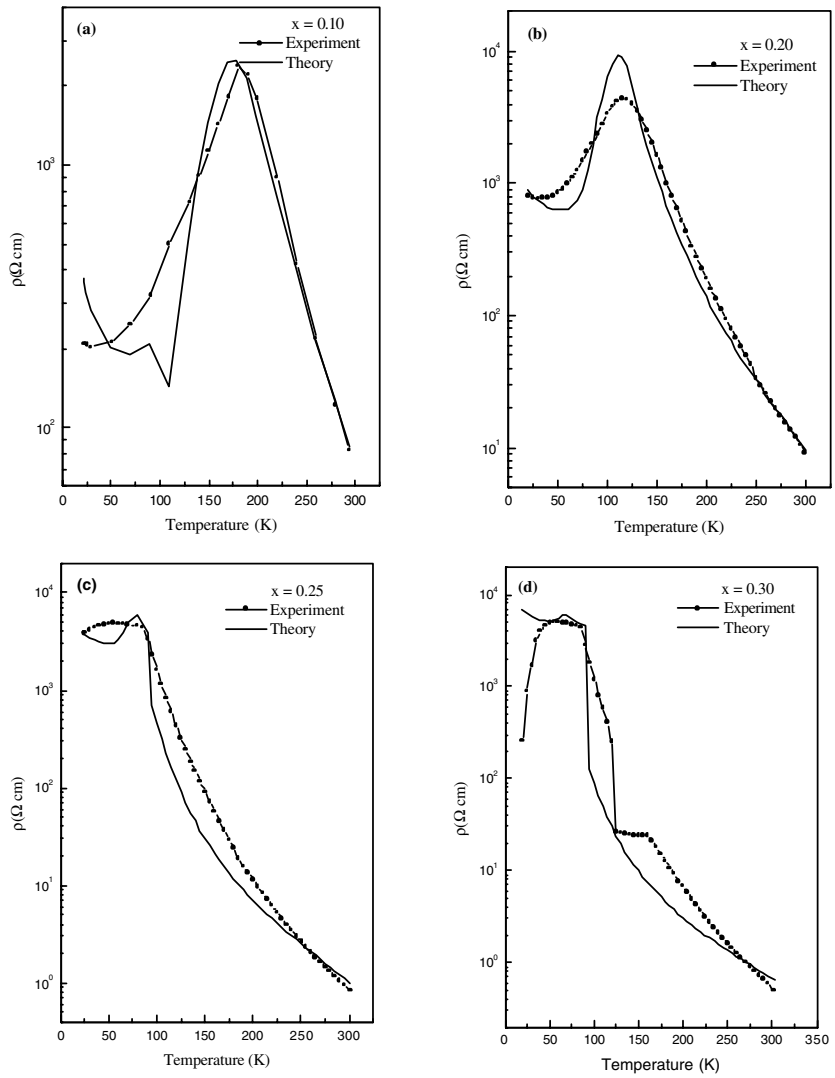

Figure 4. The comparison of the theoretical curve obtained from equation (3) with the experimental curves in figure 1 of the variation of resistivity with temperature for (a) $x = 0.1$, (b) $x = 0.2$, (c) $x = 0.25$, (d) $x = 0.3$, (e) $x = 0.4$ and (f) $x = 0.5$. The parameters used are given in table 1. The magnitude of ρ_{0A} indicates approximately the additional contribution to resistivity from the scattering by Co atoms at low temperature below $T_c' = 90$ K (see the text).

$\varepsilon_p' = 60$ K and $m(t') = 1$. Other parameters that fit the data are given in table 1. We show in figures 4(a)–(f) the calculated $\bar{\rho}$ versus T curve for $0.1 \leqslant x \leqslant 0.5$ from equation (3).

The special features of $\rho(T)$ discussed in section 3.1 are accounted for by equation (3). The room temperature resistivity of $x = 0.1$ is two orders of magnitude larger than $x = 0.25$ since the number of charge carriers is 10^{18} cm^{-3} in the former and 10^{20} cm^{-3} in the latter. The number of charge carriers is a sensitive function of the commensurate fraction, $N/8$, of the cobalt concentration. For $x < 0.25$, the Co ion is randomly distributed on the lattice and so both the number of mobile charges and mobility, μ, in $\rho = (ne\mu)^{-1}$ are small. Only when

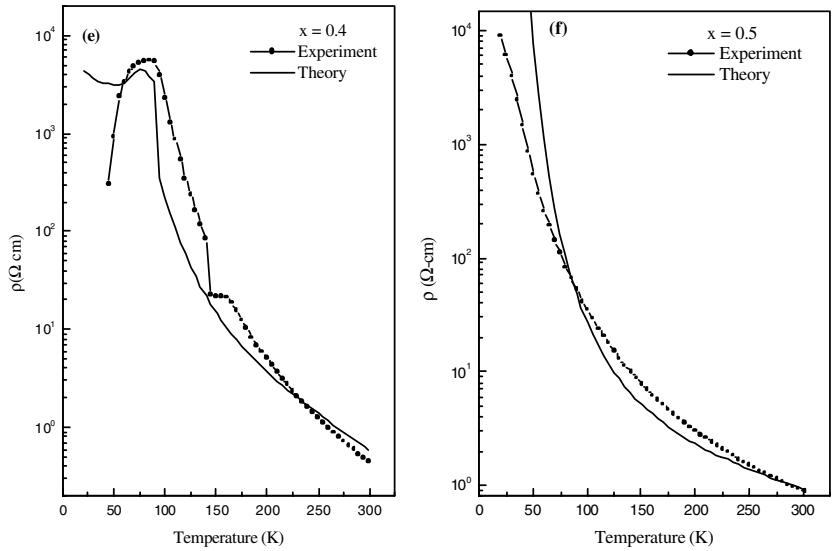

Figure 4. (Continued.)

x reaches 0.25 ($N = 2$) does an ordered AFM-A phase precipitate and coexist with the FM-B type phase. In that case n increases by two orders of magnitude and U_0 decreases from 1150 to 800 K (table 1). This is indicated in figure 3 where for $0.1 \leqslant x < 0.2$ only a single magnetic phase FM-B is shown to exist with cobalt acting as random impurity. When cobalt orders at $x = 0.25$, AFM-A precipitates and n steeply increases while U_0 decreases. The upturn at low temperature in resistivity for $x = 0.1$ and 0.2 is due to the two cosh terms and the one in equation (1) dominates since $\varepsilon_p = 400$ K while $\varepsilon'_p = 60$ K. For $x > 0.2$ ε_p reduces to 200 K so the contribution from the A-type scattering dominates and at T_1 when the trivalent cobalt atoms become diamagnetic the magnetic scattering from these atoms ceases to exist. Further for $x = 0.3$ and 0.4 the product of the numbers of Mn^{3+} and Mn^{4+} on A_1 (B_1) and A_2 (B_2) sublattices respectively increases (table 2) resulting in a downturn in resistivity for $T < T_1$. The peak resistivity is a product of n^{-1} and $\exp(U/T)$. As n increases ε_p is decreasing so the product is nearly a constant for $0.1 \leqslant x \leqslant 0.4$. The theoretical curves are smaller in width due probably to grain size effects which have not been included in equation (1), but as discussed in [17] affect the width and the position of the peak. The calculated curve for $x = 0.5$ using equation (1) is given in figure 4(f) with parameters given in table 1. Since in this case net magnetization is small (table 2) we have taken $m = 0$ in equation (1). As stated above the curves for $x = 0.7$ and 0.9 are similar to $x = 0.5$ and hence have not been included.

4.2. Magnetization

The dependence of magnetization on x and T as shown in figures 2(a) and (b) can be understood on the basis of spin and charge order in $La_{0.7}Ca_{0.3}Mn^{3+}_{0.7(1-x)}Mn^{4+}_{0.3(1-x)}Co^{3+}_{0.7x}Co^{4+}_{0.3x}O_3$. In the magnetic unit cell with twice the cell constant a of the chemical unit cell, there are eight magnetic atoms. We assume the Ising type of spin order for the binary system of Mn and Co, both of which are in mixed valence states. As discussed in section 4.1 special features that emerge in $\rho(T)$ and $M(T)$ are related to the charge and spin ordering phenomena that appear at concentrations of $x = 0.25N$ per Co atom. At $x = 0.25$ in addition to the PI to FM metal transition at T_c near 188 K, there occurs a FM to AF II transition near T_1 in

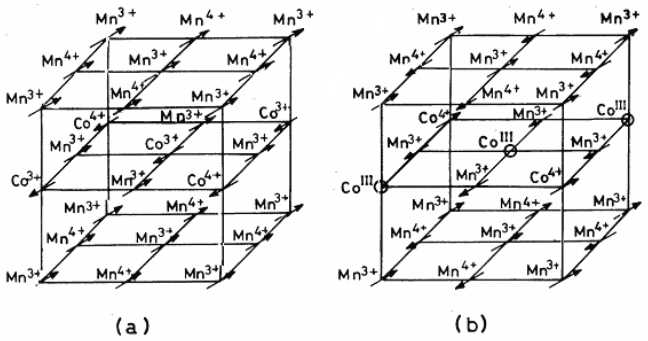

Figure 5. Spin and charge order for $x = 0.25$ in $La_{0.7}Ca_{0.3}Mn_{1-x}Co_xO_3$ (a) in the FM phase when the Co^{3+} ($S = 2$) is in the high spin state ($T_1 \leqslant T \leqslant T_c$) and (b) in the AFM phase when Co^{III} ($S = 0$) is in the low spin state ($0 \leqslant T \leqslant T_1$).

which M_s decreases from 52 emu g^{-1} at 25 K to 20 emu g^{-1} at 5 K which extrapolates to 15 emu g^{-1} at 0 K. This feature continues for $x = 0.3$ and 0.4 for which the value of $M_s(0)$ are 5 and 1.75 emu g^{-1} respectively. For $x = 0.5$, 0.7 and 0.9 the values of $M_s(0)$ are 0, 1 and 3.75 emu g^{-1} respectively. For these compositions the resistivity data show a continuous increase in resistivity as the temperature decreases from 80 to 10 K as shown in figure 1 for $x = 0.5$. For $x > 0.2$, there are two critical points (figure 3). The upper critical point occurs at T_c for $0.1 < x < 0.5$ and at T_N for $0.5 \leqslant x \leqslant 0.9$. The lower critical point occurs at $T_1 \sim 50$ K for $0.25 \leqslant x \leqslant 0.9$. The values of the peak magnetization in the FM region, M_s^p, along with the values of magnetization at 0 K, $M_s(0)$, with T_c, T_N and T_1 for $0.1 \leqslant x \leqslant 0.9$ in $La_{0.7}Ca_{0.3}Mn_{1-x}Co_xO_3$ are given in table 2. The observed values of M_s^p and $M_s(0)$ can be accounted for on the following assumption.

(i) The DE interaction occurs largely between Mn^{3+} ($t_{2g}^3e_g^1$) and Mn^{4+} ($t_{2g}^3e_g^0$) and only weakly between Co^{3+} ($t_{2g}^4e_g^2$) and Co^{4+} ($t_{2g}^4e_g^1$). Mn^{3+}, Mn^{4+} and Co^{3+} are in the high spin state and Co^{4+} is in the intermediate spin state.

(ii) The SE interaction occurs between Mn^{m+} and Co^{n+} ($m, n = 3, 4$) such that

$$|J(Mn^{m+}\text{–}Co^{n+})|S^2 > |J(Mn^{m+}\text{–}Mn^{n+})|S^2 > E^D(Mn^{3+}\text{–}Mn^{4+})$$

where E^D is the energy due to the DE interaction, $J(i)$ is the SE interaction constant and S represents the average spin of the interacting spins. This accounts for the dominance of DE over SE for $x \leqslant 0.4$ while the opposite holds for $x \geqslant 0.5$.

(iii) Below T_1, Co^{3+} changes from the high spin ($t_{2g}^4e_g^2$) to the low spin state ($t_{2g}^6e_g^0$). Since in this region the magnetic coupling due to DE is suppressed, SE dominates and the TM^{m+}–TM^{n+} interactions are AFM. Here TM are transition metal atoms.

Jadhao *et al* [14] have shown through Mossbauer spectroscopy that the energy gap between the low spin and high spin states in $EuCoO_3$ is 20 meV which is comparable to the energy difference suggested by Raccah and Goodenough for $LaCoO_3$ as $E_{Co}^{3+} - E_{Co}^{III} \leqslant 80$ meV [15]. We find that below $T_1 \sim 50$ K the Co^{3+} spins begin to change to the Co^{III} state as the latter lies lower in energy than the high spin state in $La_{0.7}Ca_{0.3}Mn_{1-x}Co_xO_3$ and at 0 K it is entirely in the low spin state.

Based on the above, possible charge and spin arrangements on sublattices A_1, A_2, B_1 and B_2 are given in table 2 for $0.1 \leqslant x \leqslant 0.9$ in $La_{0.7}Ca_{0.3}Mn_{1-x}Co_xO_3$ which accounts for M^p and $M(0)$. For $x = 0.25$ this arrangement for a magnetic unit cell is shown in figure 5(a) for

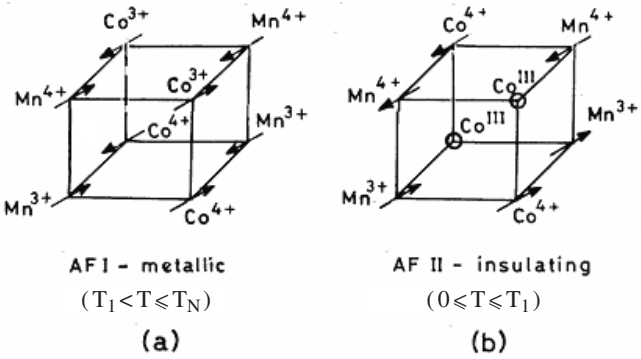

Figure 6. Spin and charge distribution for $x = 0.5$ in $La_{0.7}Ca_{0.3}Mn_{1-x}Co_xO_3$ for the (a) high spin Co^{3+} ($S = 2$) (AF I) and (b) low spin Co^{III} ($S = 0$) (AF II) phase.

the FM state when cobalt is in the high spin state Co^{3+} ($t_{2g}^4e_g^2$) and in figure 5(b) for the AFM state when it is in the low spin state Co^{III} ($t_{2g}^6e_g^0$). The estimated values of M^p and $M(0)$ are 47.29 and 14.67 emu g^{-1} which agree well with the observed values of 52 and 15 emu g^{-1} respectively (figure 2(a) and table 2). As in [16] 'A' refers to spins aligned parallel to the quantization axis Z ($+S_Z$) while 'B' refers to antiparallel alignment ($-S_Z$). The subscript '1' refers to the spins on the lattice sites (000) and (aa0) while '2' refers to the spins on sites (a00) and (aaa). The maximum number of spins on each sublattice is four. It is argued above that four Mn and Co atoms order in the magnetic unit cell for the commensurate fraction $0.25N$ of Co ions. Accordingly we notice in figure 2(a) a change in the $M(T)$ curve for $x = 0.25$. Further, in figure 3 for $x = 0.5$, the spin and charge distributions for the phases AF I and AF II (in which the trivalent Co ions are in high and low spin states respectively) are given in figures 6(a) and 6(b) for an octant.

The spin order is decided by the relative strengths of SE and DE interactions. The strength of DE is related to ε_p and can be estimated from the resistivity data. The value of ε_p for $x = 0.1$ is 400 K which is large compared to 250 K observed for $x = 0$ in [16]. As T_c for $x = 0$ is 260 K and $x = 0.1$ is 220 K, it can be taken that even for a small value of cobalt content, the SE interaction begins to increase rapidly compared to DE.

4.3. Magnetic phase diagram

The general features of the magnetic phase diagram shown in figure 3 have been discussed in section 3.3. The expression for T_c and T_N given by de Gennes [18] is used to obtain the upper critical point in the phase diagram. As discussed [16] we can write for the present system

$$k_B T_c(K) = \frac{2}{3}[z_a|J_a| - z_b|J_b| - z_c|J_c|]S^2 + \frac{0.6(1-x)z\varepsilon_p}{5} \tag{5}$$

$$k_B T_N(K) = \tfrac{2}{3}[z_a|J_a| - z_b|J_b| + z_c|J_c|]S^2 \tag{6}$$

where z_i ($i = a, b, c$) are the numbers of nearest neighbours along the a, b, c directions, z is the total number of nearest neighbours and J^i is the effective J in the i direction. Here a denotes the e_g bond direction in the ab plane, c denotes the direction of the isotropic AF $J^{t_{2g}}$ band and x denotes the concentration of the Co ion. For $x < 0.5$, DE dominates and J_a, J_b and J_c are independent of x as exchange involving e_g and t_{2g} orbitals remains unaffected by cobalt substitution. When Co concentration equals or exceeds Mn, DE involving the e_g orbital

decreases, so J_a changes without any change in J_b and J_c. We then take the following using arguments given in [16]:

$$\begin{aligned} &J_a = 3.08 \text{ meV}; \quad J_b = 0.62 \text{ meV}; \quad J_c = 0.62 \text{ meV} \quad \text{for } x < 0.5 \\ &J_a = (3.08 - 4.92(x - 0.5)) \text{ meV}; \quad J_b = 0.62 \text{ meV}; \quad J_c = 1.15 \text{ meV} \quad \text{for } x \geqslant 0.5. \end{aligned} \tag{7}$$

As argued by de Gennes [18], in such a case the upper transition point is given by the greater of the two quantities quoted in equations (5) and (6). A plot of T_c and T_N as a function of x using equations (5) and (6) and $z = 6$, $S = 1.75$ and ε_p values given in table 1 is given in figure 3. This shows that the FM phase is stable for $x < 0.25$ and the AFM phase is stabilized for $x \geqslant 0.5$ as observed. The lower transition temperature T_1 occurs due to the change from the high spin to the low spin state and depends on the difference between the energies of the Co ions in the two spin states in the crystal field, $\Delta E = (E^{3+}_{\text{Co}} - E^{\text{III}}_{\text{Co}})$. As T_1 lies between 20 and 50 K in the present system $\Delta E \sim 10$ meV as suggested for $LaCoO_3$ by some investigators [14]. The agreement between theory and experiment proves the prediction of de Gennes [18] that the system adopts the B type or A type of spin order depending on the relative strength of the DE and SE which is a function of the number of mobile carriers.

Based on the magnetic and transport data the phase diagram in figure 3 is drawn and shows the existence of three regions: (i) $0.1 \leqslant x < 0.2$; (ii) $0.2 \leqslant x < 0.5$ and (iii) $0.5 \leqslant x \leqslant 0.9$. In (i) in the range $0 \leqslant T \leqslant T_c$ only the B-type FM phase exists, in (ii) in the range $T_1 < T \leqslant T_c$, both B-type FM and A-type AFM phases coexist and at low temperatures below T_1 the trivalent cobalt is in the low spin state, and in (iii) in the range $T_1 < T \leqslant T_N$ only the A-type AFM phase exists with low spin cobalt below T_1. The magnetic phase diagram is thus accounted for satisfactorily on the basis of de Gennes theory with the exchange constants given in equation (7).

5. Conclusion

The effect of cobalt substitution in $La_{0.7}Ca_{0.3}MnO_3$ (LCMO) on the transport and magnetic properties of the magnetic compound has been investigated. It is found that even 10% of cobalt in pure LCMO increases the peak resistivity near T_c^p by four orders of magnitude and decreases T_c by 15% from 260 to 220 K. As cobalt concentration increases T_c^p decreases and reaches a minimum of 75 K at $x = 0.3$. On the other hand T_c measured from magnetic data does not change much. The increase in resistivity on cobalt substitution is due to the large decrease in the density of charge carriers ($\sim 10^{-2}$), as well as in mobility since the activation energy, U_0, increases by a factor of five on 10% of cobalt substitution in pure LCMO. It is shown that in accordance with the prediction of de Gennes the layered spin system changes from the FM B to the A type of spin arrangement as the concentration of mobile charge carriers decreases and reaches a critical value. This occurs in the present system at 50% of Co concentration. The experimental upper critical point satisfies the expression derived for the Curie (T_c) and Neel (T_N) points by de Gennes for the FM (B) and AFM (A) types of spin arrangement respectively. The lower critical point, T_1, arises from the transition of cobalt trivalent ions from the high spin to the low spin state. The charge and spin distributions of manganese and cobalt ions which account for the observed peak magnetization in the FM phase and the magnetization at 0 K have been obtained for the three different phases, A, B and the low spin cobalt state in the magnetic unit cell.

Acknowledgments

We are grateful to the Department of Science and Technology for support of the project and to Saket Asthana for help in the preparation of the manuscript.

References

[1] Zener C 1951 *Phys. Rev.* **82** 403
[2] Goodenough J B 1955 *Phys. Rev.* **100** 564
[3] von Helmolt R, Wecker J, Holzapfel B, Schultz L and Samwer K 1993 *Phys. Rev. Lett.* **71** 2331
[4] Jonker G H and Van Santen J H 1950 *Physica* **16** 599
[5] Kawano H, Kajimoto R, Yoshizawa H, Tomioka Y, Kuwahara H and Tokura Y 1997 *Phys. Rev. Lett.* **78** 4253
[6] Mahesh R, Mahendiran R, Raychaudhury A K and Rao C N R 1995 *J. Solid State Chem.* **114** 297
[7] Fontcuberta J, Balcells L, Martinez B and Obradors X 1998 *Phys. Rev.* B **58** R14697
[8] Vanitha P V, Singh R S, Natarajan S and Rao C N R 1999 *Solid State Commun.* **109** 135
[9] Bahadur D, Foldeaki M, Mandal S K, Yewondwossen M H, Koizol Z and Dunlap R A 1997 *J. Alloys Compounds* **256** 76
[10] Millis A J, Shraiman B I and Mueller R 1996 *Phys. Rev. Lett.* **77** 175
[11] Pérez J, García J, Blasco J and Stankiewicz J 1998 *Phys. Rev. Lett.* **80** 2401
[12] Sun Y, Tong W, Xu X and Zhang Y 2001 *Phys. Rev.* B **63** 174438
[13] Raveau B, Maignan A and Martin C 1997 *J. Solid State Chem.* **130** 162
[14] Jadhao V G, Singru R M, Rao G N, Bahadur D and Rao C N R 1975 *J. Phys. Chem. Solids.* **37** 113
[15] Raccah P M and Goodenough J B 1967 *Phys. Rev.* **155** 932
[16] Srivastava C M 1999 *J. Phys.: Condens. Matter* **11** 4539
[17] Das R N, Das D, Srivastava C M, Nigam A K, Chowdhury P and Bahadur D 2000 *Ferrites: Proc. 8th Int. Conf. on Ferrites (ICF 8) (Kyoto and Tokyo, Japan 250)*
[18] de Gennes P G 1960 *Phys. Rev.* **188** 141